ligands are larger than in **6a** (**6b**; Cp_c–Co 1.670 Å; Cbd_c–Co 1.692 Å) and close to those found for the parent system.[13] The new protocol reported herein for the synthesis of endohedral metallocenophanes has several advantages: it is not limited to stable cyclophanes as starting materials, and the length of the bridges and their substitution pattern on the first ligand are variable.

Received: February 9, 2001 [Z16591]

[1] Review: J. Schulz, F. Vögtle, *Top. Curr. Chem.* **1994**, *172*, 41.

[2] Reviews: R. L. Halterman in *Metallocenes: Synthesis, Reactivity, Applications*, *Vol. 1* (Eds.: A. Togni, R. L. Halterman), Wiley-VCH, Weinheim, **1998**, p. 455; R. L. Halterman, *Chem. Rev.* **1992**, *92*, 965.

[3] A. Lüttringhaus, W. Kullik, *Angew. Chem.* **1958**, *70*, 438; K. Hafner, C. Mink, H.-J. Lindner, *Angew. Chem.* **1994**, *106*, 1566; *Angew. Chem. Int. Ed. Engl.* **1994**, *33*, 1479; S. Miyake, L. M. Henling, J. E. Beslaw, *Organometallics* **1998**, *17*, 5328.

[4] C. Elschenbroich, R. Möckel, U. Zenneck, *Angew. Chem.* **1978**, *90*, 560; *Angew. Chem. Int. Ed. Engl.* **1978**, *17*, 531; A. R. Koray, M. L. Ziegler, N. E. Blank, M. W. Haenel, *Tetrahedron Lett.* **1979**, *26*, 2465.

[5] Review: H. Schmidbaur, *Angew. Chem.* **1985**, *97*, 893; *Angew. Chem. Int. Ed. Engl.* **1985**, *24*, 893; P. Jutzi, R. Krallmann, G. Wolf, B. Neumann, H. G. Stammler, *Chem. Ber.* **1991**, *124*, 2391.

[6] Review: M. Hisatome, *Rev. Heteroat. Chem.* **1992**, *6*, 142; M. Hisatome, J. Watanabe, K. Yamakawa, *Bull. Chem. Soc. Jpn.* **1994**, *67*, 280.

[7] C. Ruangstayanand, H.-J. Rimek, F. Zymalkowski, *Chem. Ber.* **1970**, *103*, 2403.

[8] K. Ishii, T. Nakano, T. Zenko, M. Kotera, M. Sakamoto, *J. Chem. Soc. Perkin Trans. 1* **1991**, 2057.

[9] The chloroalkynes were prepared analogously to those reported by J. White, C. G. Whiteley, *Synthesis* **1993**, 1141.

[10] W. P. Hart, D. W. Macomber, M. D. Rausch, *J. Am. Chem. Soc.* **1980**, *102*, 1196.

[11] Most relevant analytical data of **5**–**7**: **5a** ^{1}H NMR (500 MHz, C_6D_6): $\delta = 1.24$ (s, 18H), 1.46–1.52 (q, 4H), 2.01–2.08 (m, 8H), 4.48 (s, 2H), 4.61 (s, 1H); ^{13}C NMR (125 MHz, C_6D_6): $\delta = 18.7$ (CH_2), 27.4 (CH_2), 27.6 (C), 30.3 (CH_2), 31.6 (CH_3), 78.1 (C), 83,6 (CH), 85.6 (CH), 90.0 (C), 105.4 (C). **5b**: ^{1}H NMR (300 MHz, C_6D_6): $\delta = 1.22$ (s, 18H), 1.29–1.43 (m, 8H), 1.85–1.90 (m, 4H), 1.99–2.04 (m, 6H), 4.49 (2H), 4.61 (1H); ^{13}C NMR (75 MHz, C_6D_6): $\delta = 18.8$ (CH_2), 27.6 (C), 27.9 (CH_2), 29.1 (CH_2), 30.0 (CH_2), 31.6 (CH_3), 78.4 (C), 83.4 (CH), 85.4 (CH), 89.4 (C), 105.9 (C). **5c**: ^{1}H NMR (300 MHz, C_6D_6): $\delta = 1.12$–1.91 (m, 28H), 2.06 (m, 4H), 2.08 (m, 6H), 4.50 (s, 2H), 4.60 (s, 1H); ^{13}C NMR (75 MHz, C_6D_6): $\delta = 18.7$ (CH_2), 27.3 (C), 28.1 (CH_2), 28.5 (CH_2), 28.9 (CH_2), 30.3 (CH_2), 31.4 (CH_3), 78.5 (C), 83.2 (CH), 85.3 (CH), 89.0 (C), 105.8 (C). **6a**: yellow solid, m.p. 95 °C; ^{1}H NMR (300 MHz, C_6D_6): $\delta = 1.13$ (s, 9H), 1.22 (s, 9H), 1.58–1.75 (m, 8H), 1.94–1.98 (m, 2H), 2.29–2.35 (m, 2H), 4.63 (s, 2H), 5.33 (s, 1H); ^{13}C NMR (125 MHz, C_6D_6): $\delta = 22.7$ (CH_2), 24.3 (CH_2), 31.3 (CH_3), 32.5 (CH_3), 32.6 (C), 33.4 (C), 41.6 (CH_2), 66.4 (C), 82.2 (CH), 85.7 (CH), 91.9 (C), 94.9 (C), 100.7 (C); HR-MS (positive ions) calcd for $C_{23}H_{33}Co$: 368.1914; found: 368.1904. **6b**: yellow solid, m.p. 135 °C; ^{1}H NMR (300 MHz, C_6D_6): $\delta = 1.25$ (s, 9H), 1.30 (s, 9H), 1.51–1.72 (m, 8H), 2.13–2.17 (m, 4H), 2.25–2.33 (m, 2H), 2.62–2.69 (m, 2H), 4.84 (s, 3H); ^{13}C NMR (75 MHz, C_6D_6): $\delta = 28.3$ (CH_2), 28.5 (CH_2), 29.9 (CH_2), 31.7 (CH_2), 31.9 (CH_3), 32.0 (C), 32.9 (C), 33.1 (CH_3), 70.3 (C), 79.1 (CH), 81.4 (CH), 90.5 (C), 90.8 (C), 95.1 (C); HRMS (positive EI) calcd for $C_{25}H_{37}Co$: 396.2227; found: 396.2229. **6c** + **7**: yellow solid; ^{1}H NMR (300 MHz, C_7D_8): $\delta = 1.16$ (s, 9H), 1.17 (s, 9H), 1.26 (s, 18H), 1.73–1.30 (br, 18H), 2.03–1.75 (br, 10H), 2.73–2.21 (br, 12H), 4.48 (s, 1H), 4.72 (s, 4H), 4.89 (s, 1H); ^{13}C NMR (125 MHz, C_6D_6): $\delta = 22.5$ (CH_2), 23.6 (CH_2), 23.9 (CH_2), 24.2 (CH_2), 24.3 (CH_2), 24.9 (CH_2), 24.9 (CH_2), 25.4 (CH_2), 26.1 (CH_2), 30.2 (CH_2), 30.8 (CH_3), 31.5 (C), 31.6 (CH_3), 31.8 (C), 32.4 (C), 32.9 (CH_3), 74.0 (C), 77.0 (C), 77.2 (CH), 77.3 (CH), 79.4 (CH), 83.5 (CH), 85.7 (C), 85.8 (C), 88.3 (C), 94.6 (C), 96.7 (C); HR-MS (positive ions) calcd for $C_{27}H_{41}Co$: 424.2540; found: 424.2537.

[12] X-ray analysis of **6a**: $C_{23}H_{33}Co$, $M_r = 368.42$, monoclinic, space group $P2_1/c$, crystal dimensions: $0.36 \times 0.20 \times 0.08$ mm^3, $a = 14.0457(1)$, $b = 9.9803(1)$, $c = 14.3919(2)$ Å, $\beta = 103.97(1)^\circ$, $V = 1957.72(4)$ Å^3, $Z = 4$, $T = 200(2)$ K, $\rho_{calcd} = 1.25$ g cm^{-3}, Bruker Smart CCD, $Mo_{K\alpha}$ radiation, 19646 reflections collected, 4474 unique reflections ($R_{int} = 0.0446$), 3451 observed reflections with $I > 2\sigma(I)$, an empirical absorption correction was applied by using SADABS,[14] based on the Laue symmetry of the reciprocal space, $\mu = 0.88$ mm^{-1}, $T_{min} = 0.74$, $T_{max} = 0.94$. The structure was solved by the Patterson method and refined against F^2 with a full-matrix least-squares algorithm by using the SHELXTL (5.1) software package,[15] 223 parameters refined, $R1 = 0.034$, $wR2 = 0.073$ ($I > 2\sigma(I)$), GOF = 1.04. The maximum and minimum residual electron density is 0.28 and -0.35 e Å^{-3}, respectively. X-ray analysis of **6b**: $C_{25}H_{37}Co$, $M_r = 396.48$, orthorhombic, space group $Pna2_1$, crystal dimensions: $0.58 \times 0.42 \times 0.24$ mm^3, $a = 10.3000(1)$, $b = 13.5018(1)$, $c = 15.0996(1)$ Å, $V = 2099.88(3)$ Å^3, $Z = 4$, $T = 200(2)$ K, $\rho_{calcd} = 1.25$ g cm^{-3}, Bruker Smart CCD, $Mo_{K\alpha}$ radiation, 15308 reflections collected, 3098 unique reflections ($R_{int} = 0.0812$), 2306 observed reflections with $I > 2\sigma(I)$, an empirical absorption correction was applied by using SADABS,[14] based on the Laue symmetry of the reciprocal space, $\mu = 0.82$ mm^{-1}, $T_{min} = 0.65$, $T_{max} = 0.86$. The structure was solved by direct methods and refined against F^2 with a full-matrix least-squares algorithm by using the SHELXTL (5.1) software package,[15] 241 parameters refined, $R1 = 0.037$, $wR2 = 0.068$ ($I > 2\sigma(I)$), GOF = 0.96. The maximum and minimum residual electron density is 0.72 and -0.29 e Å^{-3}, respectively. The crystallographic data (excluding structure factors) for the structures reported herein have been deposited with the Cambridge Crystallographic Data Centre as supplementary publication no. CCDC-161078 (**6a**) and CCDC-161079 (**6b**). Copies of the data can be obtained free of charge on application to CCDC, 12 Union Road, Cambridge CB21EZ, UK (fax: (+44) 1223-336-033; e-mail: deposit@ccdc.cam.ac.uk).

[13] P. E. Riley, R. E. Davis, *J. Organomet. Chem.* **1976**, *113*, 157.

[14] G. M. Sheldrick, 1996, unpublished work based on the method described in R. H. Blessing, *Acta Crystallogr. Sect. A* **1995**, S1, S33.

[15] G. M. Sheldrick, Bruker Analytical X-ray-Division, Madison, WI, **1997**.

Low-Temperature Selective Catalytic Reduction (SCR) of NO with NH_3 by Using Mn, Cr, and Cu Oxides Supported on Hombikat TiO_2**

Panagiotis G. Smirniotis,* Donovan A. Peña, and Balu S. Uphade

Nitrogen oxides are man-made pollutants, emitted from mobile and stationary sources, that greatly contribute to the formation of smog, acid rain, and ozone. Automobiles are the primary mobile sources of NO_x emissions, while the stationary sources consist of oil and coal-fired power stations and nitric acid production plants. The direct health hazards related to NO_x are bronchitis, pneumonia, viral infections, and hay fever. Selective catalytic reduction (SCR) of NO with ammonia in the presence of oxygen [Eq. (1)] is the proven technology for

$$4\,NO + 4\,NH_3 + O_2 \longrightarrow 4\,N_2 + 6\,H_2O \quad (1)$$

[*] Prof. P. G. Smirniotis, D. A. Peña, B. S. Uphade
Chemical Engineering Department
University of Cincinnati
Cincinnati, OH 45221-0171 (USA)
Fax: (+1) 513-556-3473
E-mail: Panagiotis.Smirniotis@UC.EDU

[**] We are grateful to the Ohio Coal Development Office (OCDO), Columbus, Ohio, for financial support and for allowing us to publish the findings.

effective removal of NO_x from stationary sources.[1] A process based on V_2O_5/TiO_2[2–6] catalysts with or without the addition of either WO_3 or MoO_3 was developed and successfully commercialized for NO_x removal (catalysts for NO_x removal are known as DeNOx catalysts). The system is successful because of its high activity and resistance to SO_2 poisoning. However, the main disadvantage of this type of catalyst is that it does not work at reaction temperatures $\leq 250\,^{\circ}C$. The other disadvantages include over-oxidation of NH_3 to N_2O and NO and the oxidation of SO_2 to SO_3. There is an urgent need for the development of low-temperature SCR methods for the treatment of flue gas, especially from electric power plants, shaft furnaces, and waste incinerators. Large quantities of NO_x are generated at such sites, and the flue-gas temperature at the outlet of the heat-recovery system or smokestack is normally $\leq 150\,^{\circ}C$.

Platinum-based catalysts were found to be highly active for the reaction in Equation (1), however, the scarcity of Pt, the oxidation of NH_3 to NO_x at relatively high temperature, high cost, and rapid poisoning under stack-gas conditions have prompted worldwide efforts to develop low-cost supported metal or mixed metal oxide catalysts. Metal oxides, such as MoO_3,[7] CuO, and MnO_x,[8, 9] supported on TiO_2, Al_2O_3, or activated carbon fibers have been reported to be active for the SCR process at temperatures greater than $300\,^{\circ}C$, however, the high temperature results in poor N_2 selectivity. Recently, a highly active and SO_2 resistant activated-carbon-supported V_2O_5 catalyst was reported,[10] however, it is active only above $150\,^{\circ}C$ and also needs specific pretreatment for initial activation. Additionally, the stability of carbon-containing catalysts in O_2 is low.

Herein we show that transition metal oxides supported on Hombikat TiO_2 display substantial activity for NO reduction and also a 100% yield of N_2 at much lower reaction temperatures ($\leq 120\,^{\circ}C$, Table 1); to our knowledge, these catalytic results are the best reported so far. Of the catalysts we studied, the best results were obtained over the Mn on Hombikat TiO_2 catalyst. The catalyst characterization and activity data obtained at $100\,^{\circ}C$ and $120\,^{\circ}C$ for various transition metal oxides deposited on different supports are given in Table 1. From X-ray diffraction (XRD) studies only weak peaks arising from transition metal oxides were obtained, suggesting that the catalysts are mostly amorphous. Surprisingly the observed metal dispersion for our best catalyst was poor even on a high-surface-area support, indicating that high metal dispersion is not crucial. Noteworthy is that catalysts containing metals other than Mn, Cr, and Cu are far less active; the multivalent nature of Mn, Cr, and Cu oxides may facilitate the redox activity of the catalysts.

Consistent with the literature data,[11] our Cr/TiO_2 catalyst also produced undesired N_2O which indicates the possible presence of CrO_2, however, this phase was not detected in our XRD analysis. Ni on Hombikat TiO_2 shows no activity, which is attributed to the confined monovalent oxidation state of nickel and also the low surface concentration of nickel observed from X-ray photoemission spectroscopy (XPS). Our XPS data confirmed that the Mn/Hombikat TiO_2 system has the greatest metal oxide surface concentration (Table 1). This result suggests that more MnO_x species are available to participate in the reaction, which may explain the excellent performance of the Mn/Hombikat TiO_2 catalyst. Deconvoluted XPS spectra for Mn $2p_{3/2}$ indicate the presence of MnO_2 (642.2 eV) as the major phase and Mn_2O_3 (641.2 eV) as a minor phase along with a third phase, possibly partially undecomposed manganese nitrate (643.8 eV) resulting from the relatively low calcination temperature. The binding-energy values match well with the literature values.[12] The results suggest the possibility of redox behavior during the catalytic reaction.

A Fourier Transform infrared (FT-IR) spectroscopy study of NH_3 shows that the Brønsted:Lewis acid site ratio for the Mn/Hombikat TiO_2 system is lower than that of the other catalysts (see Table 1). In contrast, V/Hombikat TiO_2, which resembles a typical medium-temperature DeNOx catalyst, shows a large number of Brønsted ($1421\ cm^{-1}$) rather than Lewis ($1607\ cm^{-1}$) acid sites. These results clearly indicate that Lewis acidity is more important than Brønsted acidity for low-temperature SCR catalysts. The NH_3 FT-IR results are

Table 1. Catalyst characterization, activity data, and comparison with literature results involving commercial catalysts.

Support	Transition metal	Surface area [$m^2 g^{-1}$]		Metal dispersion [%]	M2p/M′2p[l]	Crystal phases[m]	Total acidity [$\mu mol\,g^{-1}$]	[n]	NO conversion (%) at	
		support	catalyst						100 °C	120 °C
TiO_2[a]	V	309	51	12.2	0.4	V_2O_5, V_2O_4	9.8	6.09	10	19
TiO_2[a]	Cr	309	143	10.4	0.6	CrO_2, Cr_2O_3	55.8	0.11	80	91
TiO_2[a]	Mn	309	204	8.9	6.0	MnO_2, Mn_2O_3	23.2	0.07	82	100
TiO_2[a]	Ni	309	163	40.4	0.1	NiO	42.7	0.11	0	4
TiO_2[a]	Cu	309	140	47.2	–	CuO, Cu_2O	12.5	0.21	56	95
TiO_2[b]	Mn	53	52	7.3	0.2	MnO_2, Mn_2O_3	15.2	0.59	67	96
TiO_2[c]	Mn	9	14	7.0	0.5	MnO_2, Mn_2O_3	1.1	0.76	38	64
SiO_2[d]	Mn	559	421	7.0	0.8	MnO_2, Mn_2O_3	5.9	0.24	57	93
γ-Al_2O_3[e]	Mn	205	180	6.8	3.4	MnO_2, Mn_2O_3	31.0	0.40	56	89
1.4% w/w V_2O_5, 9.0% w/w WO_3/TiO_2[f] (a catalyst similar to a commercial DeNOx catalyst)[f][14]								–	12[g]	98[h]
NO_xCAT920LT (a Pt based commercial catalyst)[i][15]							–	–	63[j]	91[k]

[a] Hombikat, [b] Degussa P25, [c], [d] Aldrich, [e] Puralox, M = V, Cr, Mn, Ni, Cu; M′ = Ti, Si, Al, [f] experimental conditions: catalyst weight 160 mg, p = 1 atm, flow rate $60\ cm^3\,min^{-1}$; feed He with 800 ppm each of NH_3 and NO and 1 vol% O_2, [g] at $150\,^{\circ}C$ and 98% N_2 selectivity, [h] at $300\,^{\circ}C$ and 98% N_2 selectivity, [i] experimental conditions: N_2 with 500 ppm NO, 400 ppm NH_3, and 4 vol% O_2, GHSV = 24000 h^{-1}, [j] at $180\,^{\circ}C$ and 45% N_2 selectivity, [k] at $240\,^{\circ}C$ and 35% N_2 selectivity, [l] emission intensity ratios from XPS measurements of surface elemental composition, [m] from XRD and XPS measurements, [n] ratio of Brønsted to Lewis acid centers.

  1433-7851/01/4013-2480 $ 17.50+.50/0

consistent with those reported by Busca and co-workers.[13] The NO conversion improved with increased Mn loading of the Hombikat TiO_2, and can be attributed to the increased surface concentration of Mn (determined by XPS; Table 1). 20 wt% Mn/Hombikat TiO_2 tested over a broad temperature range (80–180 °C) showed only trace amounts of N_2O (<5%) at 180 °C. In addition this catalyst showed no decrease in activity after 50 h on stream at 120 °C.

The activity of Mn-, Cr-, and Cu-loaded Hombikat TiO_2 catalysts was compared with the commercial V_2O_5/TiO_2[14] and noble metal[15] based catalysts (Table 1). Although the results on the commercial catalysts were not collected under identical experimental conditions, they do demonstrate the superior performance of our catalysts over both the commercial catalysts. High catalytic activity of our catalysts at low temperature is attributed to the redox behavior of the metal oxides, the high surface concentration of transition metal oxides, and Lewis acidity.

Any SCR catalyst intended for commercial application should be tested in the presence of water and at space velocities close to industrial scale. Our best catalyst, 20 wt% Mn/Hombikat TiO_2, showed excellent results (Figure 1) at

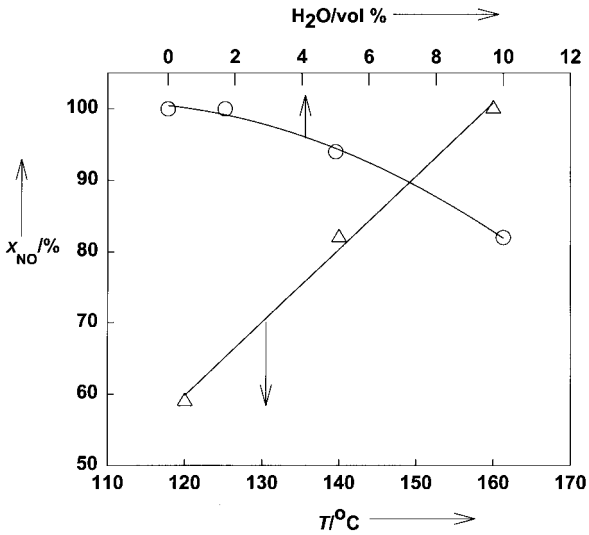

Figure 1. Influence of inlet water concentration on NO conversion in the SCR reaction over 20 wt% Mn/Hombikat TiO_2 at different temperatures, feed: NO = NH_3 = 2000 ppm, O_2 = 2 vol%, He carrier gas, H_2O = 1.7–10 vol%, catalyst = 0.1 g, total flow = 17.3 mL min^{-1}. △ = 1.7 vol% H_2O, ○ = 160 °C.

120–180 °C with inlet water concentrations as high as 10 vol%, indicating very good hydrothermal stability. Less than 3% N_2O formation was detected at 180 °C. These results are superior to those in the literature. The same catalyst was also tested in a wide gas hourly space velocity (GHSV) range (4000 h^{-1} to 64000 h^{-1}). The results (Figure 2) show an approximate 50% decrease in NO conversion at higher GHSV. However, it should be noted that we have used higher levels of NO (2000 ppm) in the feed than that found in coal-fired power plants (400–500 ppm).

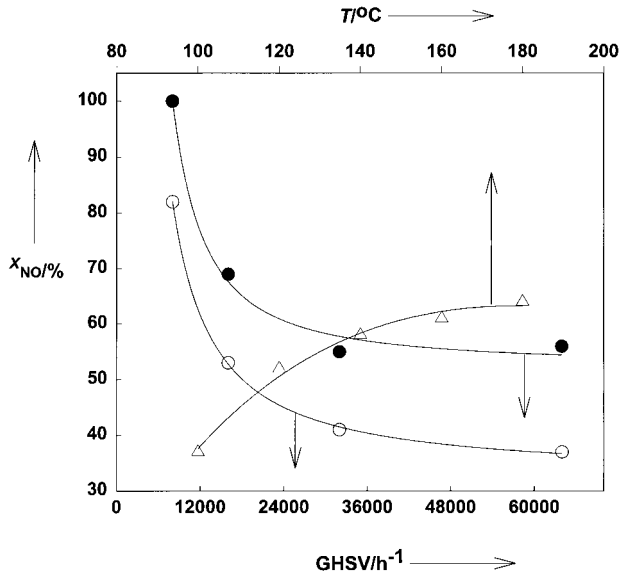

Figure 2. Influence of GHSV on NO conversion in the SCR reaction at different temperatures over 20 wt% Mn/Hombikat TiO_2 feed: NO = NH_3 = 2000 ppm, O_2 = 2 vol%, He carrier gas, catalyst = 0.1 g, total flow = 17.3 mL min^{-1}, ○ = 120 °C, ● = 140 °C, △ = 64000 h^{-1}.

In conclusion, a new highly active, time-stable, and water resistant catalyst operating at low temperature (80–180 °C) has been developed for the SCR of NO with NH_3 in excess O_2. Further studies are in progress to better understand the mechanistic aspects of our catalytic system.

Experimental Section

Transition metal oxides were deposited on various supports (Table 1) using aqueous solutions of metal nitrates. In a typical synthesis, distilled water (50 mL) was added to a 100 mL beaker containing the support (1.0 g). The mixture was heated to 70 °C under continuous stirring. A measured quantity of metal nitrate was added, and the mixture was evaporated to dryness. The paste obtained was further dried overnight at 110 °C, ground and sieved (80 mesh). Prior to the catalytic experiments, the catalysts were activated in situ by passing oxygen (4.18% in He) for 2 h at 400 °C. The SCR of NO at atmospheric pressure was carried out in a fixed-bed ceramic aluminum oxide reactor (internal diameter 6 mm) containing catalyst (0.1 g; 80 mesh). Oxygen (Wright Bros., 4.18% in He), ammonia (Matheson, 3.89% in He) and nitric oxide (Air Products, 2.0% in He) were used as received. The inlet concentrations of NO and NH_3 were 2000 ppm, whereas the O_2 concentration was 20000 ppm. The total flow of inlet gases was set at 17.3 mL min^{-1} to achieve a GHSV of 8000 h^{-1}. The reaction temperature was measured by a type K thermocouple inserted directly into the catalyst bed. The reactants and products were analyzed on-line using a mass spectrometer. Catalysts calcined at 400 °C for 2 h were used for XRD, NH_3 FT-IR, XPS and NH_3 temperature-programmed desorption (TPD).

Received: June 19, 2000
Revised: March 12, 2001 [Z15282]

[1] H. Bosch, F. Janssen, *Catal. Today* **1988**, *2*, 369–531.
[2] M. Inomata, A. Miyamoto, Y. Murakami, *J. Catal.* **1980**, *62*, 140–148.
[3] F. Janssen, F. van den Kerkhof, H. Bosch, J. R. H. Ross, *J. Phys. Chem.* **1987**, *91*, 5921–5927.
[4] J. A. Odriozola, J. Soria, G. A. Somarjai, H. Heinemann, J. F. Garcia de la Banda, M. Lopez Granados, J. C. Conesa, *J. Phys. Chem.* **1991**, *95*, 240–246.

  1433-7851/01/4013-2481 $ 17.50+.50/0

[5] S. C. Wood, *Chem. Eng. Prog.* **1994**, *90*, 32 – 38.
[6] J. A. Dumesic, N.-Y. Topsøe, H. Topsøe, T. Slabiak, *J. Catal.* **1996**, *163*, 409 – 417.
[7] M. de Boer, A. J. van Dillen, D. C. Koningsberger, F. J. J. G. Janssen, T. Koerts, J. W. Geus, *Stud. Surf. Sci. Catal.* **1992**, *72*, 133 – 145.
[8] L. Singoredjo, R. Korver, F. Kapteijn, J. Moulijn, *Appl. Catal. B* **1992**, *1*, 297 – 316.
[9] M. Yoshikawa, A. Yasutake, I. Mochida, *Appl. Catal. A* **1998**, *173*, 239 – 245.
[10] Z. Zhu, Z. Liu, S. Liu, H. Niu, *Appl. Catal. B* **1999**, *23*, L229 – L233.
[11] H. Schneider, M. Maciejewski, K. Köhler, A. Wokaun, A. Baiker, *J. Catal.* **1995**, *157*, 312 – 320.
[12] F. Kapteijn, A. D. van Langeveld, J. A. Moulijn, A. Andreïni, M. A. Vuurman, A. M. Turek, J.-M. Jehng, I. E. Wachs, *J. Catal.* **1994**, *150*, 94 – 104.
[13] J. M. G. Amores, V. S. Escribano, G. Ramis, G. Busca, *Appl. Catal. B* **1997**, *13*, 45 – 58.
[14] L. J. Alemany, L. Lietti, N. Ferlazzo, P. Forzatti, G. Busca, E. Giamello, F. Bregani, *J. Catal.* **1995**, *155*, 117 – 130.
[15] A. T. Krishnan, A. L. Boehman, *Appl. Catal. B* **1998**, *18*, 189 – 198.

Total Synthesis of Colombiasin A**

K. C. Nicolaou,* Georgios Vassilikogiannakis, Wolfgang Mägerlein, and Remo Kranich

Colombiasin A (**1**) is a novel diterpene recently isolated from a biologically active (against *Mycobacterium tuberculosis* H37Rv) extract obtained from the gorgonian octocoral, *Pseudopterogorgia elisabethae*, collected off San Andres Island, Colombia.[1] Its structure is characterized by a tetracyclic carbon framework whose periphery is decorated with four methyl groups, two carbonyl functions, two double bonds, and one hydroxy group. In addition, this unprecedented molecular architecture includes six stereogenic centers, two of which are adjacent quaternary carbon atoms. Despite the elegant spectroscopic studies that led to the structural elucidation of the colombiane skeleton, the absolute stereochemistry of colombiasin A (**1**) remains unassigned. The intrigue surrounding this natural product is heightened by a proposal suggesting elisabethin A (which was also found in *Pseudopterogorgia elisabethae*[2]) as a biogenetic precursor of **1**.[1] Here we report the total synthesis of colombiasin A (**1**) by a strategy which also delivered its C7 epimer as well as several other analogues.

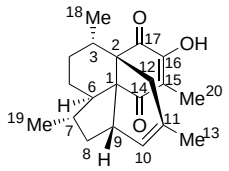

1: colombiasin A

A brief retrosynthetic analysis of colombiasin A (**1**) is presented in Scheme 1. Inspection of the target's architecture suggested quinone **A** as the cornerstone of its construction.

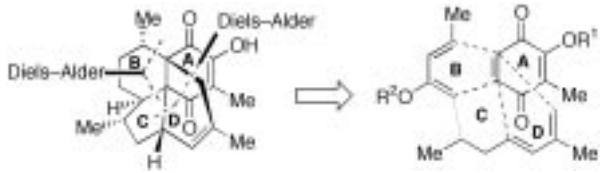

Scheme 1. Retrosynthetic analysis of colombiasin A (**1**).

Two Diels – Alder reactions, first with diene **B** (intermolecular) and then with diene **D** (intramolecular), along the sequence of elaboration, were expected to complete the polycyclic skeleton of the molecule. According to this plan, the elaboration sequence between the two cycloadditions would require both tethering of domains **B** and **D** as well as reoxidation of ring **A** to a new quinone moiety after fusion of ring **B**. To facilitate tethering of segments **B** and **D** (i.e. forming the C6–C7 bond), an oxygen-based functional group (R^2O) was temporarily incorporated into diene **B** as shown in Scheme 1. As described below, two runs of the derived strategy were necessary to reach colombiasin A (**1**).

The construction of the first key intermediate, ketone **6**, starting with the first of the projected Diels – Alder reactions is summarized in Scheme 2. Thus, reaction of diene **2** with quinone **3**[3] (obtained by *ortho*-methylation of 1,2,4-trimethoxybenzene[4] followed by oxidative demethylation[5]

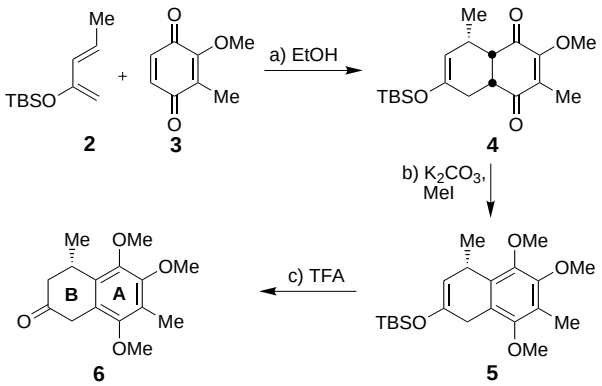

Scheme 2. Construction of **AB** ring system **6**. a) EtOH, 25 °C, 2 h, 83 %; b) K_2CO_3 (5.0 equiv), MeI (20 equiv), acetone, reflux, 48 h, 83 %; c) 2 % TFA in CH_2Cl_2, 25 °C, 2 h, 91 %. TFA = trifluoroacetic acid; TBS = *tert*-butyldimethylsilyl.

[*] Prof. Dr. K. C. Nicolaou, Dr. G. Vassilikogiannakis, Dr. W. Mägerlein, Dr. R. Kranich
Department of Chemistry and The Skaggs Institute for Chemical Biology
The Scripps Research Institute
10550 North Torrey Pines Road, La Jolla, CA 92037 (USA)
Fax: (+1) 858-784-2469
E-mail: kcn@scripps.edu
and
Department of Chemistry and Biochemistry
University of California, San Diego
9500 Gilman Drive, La Jolla, CA 92093 (USA)

[**] This work was financially supported by the National Institutes of Health (USA) and The Skaggs Institute for Chemical Biology, postdoctoral fellowships from Bayer AG (to R.K. and W.M.), and grants from Abbott, Amgen, ArrayBiopharma, Boehringer-Ingelheim, Glaxo, Hoffmann-La Roche, DuPont, Merck, Novartis, Pfizer, and Schering Plough.

  1433-7851/01/4013-2482 $ 17.50+.50/0